PCCP

Hydrogen Peroxide Generation and Hydrogen Oxidation Reactions of Vacuum-prepared Ru/Ir(111) Bimetallic Surfaces

Journal:	*Physical Chemistry Chemical Physics*
Manuscript ID	CP-ART-03-2022-001261.R1
Article Type:	Paper
Date Submitted by the Author:	29-Apr-2022

Complete List of Authors:	Hayashi, Kenta; Tohoku Daigaku, Department of Frontier Science for Advanced Environment Kusunoki, Keisuke; Tohoku Daigaku, Department of Frontier Science for Advanced Environment Tomimori, Takeru; Tohoku Daigaku, Department of Frontier Science for Advanced Environment Sato, Riku; Tohoku Daigaku, Department of Frontier Science for Advanced Environment Todoroki, Naoto; Tohoku Daigaku, Department of Frontier Science for Advanced Environment Wadayama, Toshimasa; Tohoku Daigaku, Department of Frontier Science for Advanced Environment

ARTICLE

Hydrogen Peroxide Generation and Hydrogen Oxidation Reactions of Vacuum-prepared Ru/Ir(111) Bimetallic Surfaces

Received 00th January 20xx,
Accepted 00th January 20xx

DOI: 10.1039/x0xx00000x

Kenta Hayashi,*[a] Keisuke Kusunoki,[a] Takeru Tomimori,[a] Riku Sato,[a] Naoto Todoroki,[a] and Toshimasa Wadayama[a]

From the viewpoint of the application of Ir-Ru alloys for anode of proton exchange membrane fuel cells (PEMFCs), hydrogen peroxide (H_2O_2) generation and the hydrogen oxidation reaction (HOR) properties of well-defined Ir-Ru bimetallic surfaces (Ru/Ir(111)) have been investigated using scanning electrochemical microscopy (SECM). Using thermal inter-diffusion of vacuum-deposited Ru and substrate Ir atoms, the topmost surface atomic ratios of Ru/Ir(111) were controlled via changing the substrate temperature (x) during the deposition of 1 monolayer (ML)-thick Ru. Low-energy ion scattering spectroscopy (LE-ISS) estimated the Ru/Ir ratio to be 1:1 (x = 673 K), 1:2 (x = 773 K), and 1:4 (x = 873 K). H_2O_2 generation property of Ru/Ir(111) was similar to clean Ir(111) and under the detection limit in the potential region of 0.06–0.3 V, while clean Ru(0001) generated H_2O_2 in this potential region. The results suggest the Ir sites contribute to the reduction of H_2O_2 intermediates generated at neighboring Ru sites. In contrast, the HOR activity of Ru/Ir(111) correlated with the probabilities of ensembles, such as Ir_2 dimer and Ir_3 trimer: the ensemble probabilities were calculated under assumption of randomly solute Ir and Ru atoms at the topmost surfaces. Such the close correlation suggest that the Ir ensemble sites strongly contribute to the HOR. In conclusion, the Ir sites play a key role in the suppression of H_2O_2 generation and high HOR activity, that is essential for next-generation PEMFCs anode catalysts.

Introduction

Proton exchange membrane fuel cells (PEMFCs) are a power source used for automotive applications.[1] During the normal operation of PEMFCs, the hydrogen oxidation reaction (HOR) and oxygen reduction reaction (ORR) occur at the anode and cathode, respectively, and carbon-supported Pt-based nanoparticle (Pt/C) catalysts are loaded on both electrodes to promote their respective reactions. Under the actual operating conditions of PEMFCs, however, conventional Pt-based anode catalysts trigger the chemical degradation of the proton exchange membrane (PEM) via the generation of hydrogen peroxide (H_2O_2),[2] i.e., when oxygen diffuses through the PEM from the cathode to the anode, the Pt/C catalyst generates H_2O_2 via the 2 electron pathway of ORR at low potential at the anode (~0 V vs. reversible hydrogen electrode (RHE)).[3] The generated H_2O_2 forms oxygen related radicals, which severely damage the PEM.[4] At present, although radical quenchers such as Ce^{3+} are being added to the PEM to mitigate this degradation process,[5] the inhomogeneous migration of the quencher limits the long-term stabilization.[6,7] Therefore, the development of novel anode catalysts with practical HOR activity and suppressed H_2O_2 generation is highly desirable.[8]

Ir and/or Ir alloys may be alternative materials for the PEMFC anode,[9] where Pt-based materials, such as Pt/C and Pt-Ru/C, are commonly used. Actually, the HOR activity of carbon supported Ir nanoparticles (Ir/C) has been reported to be the same order of magnitude as Pt/C,[10] and more importantly, our group recently reported the H_2O_2 generation of low-index Ir single crystal surfaces was much less than that of clean Pt(111) in the anode potential region.[11] Considering extremely high-cost and less-resource drawbacks of Ir, amount of Ir usage should be minimized; thus, Ir-based alloys are rather feasible for practical PEMFC anode, in comparison with pure Ir. In regard Ir alloys, Ir-Ru is attractive. Pak's group reported that Ir-Ru/C showed sufficient HOR activity to achieve single-cell performances comparable to those of Pt/C, and in addition, they proposed that low ORR activity and high oxygen evolution reaction activity of Ir-Ru/C are beneficial toward preventing catalyst degradation during the transient conditions of PEMFC operation, such as start-up/shutdown and cell reversal.[12–16]

Nevertheless, the detailed relationship between the alloy surface structures and catalytic properties of Ir-Ru as a PEMFC anode is elusive because of the complex alloy surface structures and compositions of the Ir-Ru/C anode catalyst. Although the HOR activity of the Ir-Ru bimetallic surface has been discussed on the basis of first-principle calculations,[17] no experimental studies using a well-defined surface of Ir-Ru alloys have been conducted to date. Furthermore, to the best of our knowledge,

[a] Graduate School of Environmental Studies, Tohoku University, Sendai 980-8579, JAPAN. *E-mail: kenta.hayashi.r8@dc.tohoku.ac.jp

Electronic Supplementary Information (ESI) available: [A: Low-energy ion scattering (LE-IS) spectrum for clean Ir(111), B: Scanning tunnelling microscopy (STM) image of the 773 K-Ru/Ir(111) surface, C: H_2O_2 generation behaviour of Ru(0001), D: Cyclic voltammograms obtained for x K-Ru/Ir(111), E: Mathematical estimation of the ensemble probability, and F: Comparison of the calculated dimer and trimer sites, and SECM-estimated HOR standard rate constant (k^0) vs. the surface Ru composition of x K-Ru/Ir(111).]. See DOI: 10.1039/x0xx00000x

the H_2O_2 generation behaviour of Ir-Ru systems has never been investigated. Therefore, in this study we have prepared well-defined Ru/Ir(111) bimetallic surfaces with different surface Ru/Ir atomic ratios. The surface structures were controlled via changing the substrate temperatures during arc-plasma deposition (APD) of Ru onto Ir(111) in a vacuum system, using the inter-diffusion and surface-segregation phenomena of constituent elements.[18,19] The H_2O_2 generation and HOR properties were then evaluated using the tip generation/substrate collection and substrate-generation/tip-collection modes in scanning electrochemical microscopy (SECM).

Experimental

Sample preparation

Ru/Ir(111) bimetallic surfaces were fabricated using a previously reported vacuum system.[18] A single-crystal of the Ir(111) substrate (MaTeck, 99.999 %, miscut angle: <0.1°) was cleaned via repeated cycles of Ar^+ sputtering and annealing at 1153 K.[11] Thereafter, one monolayer (ML)-thick Ru was deposited on the vacuum-cleaned Ir(111) surface using APD (ULVAC-RIKO, ARL-300) at different substrate temperatures (x = 673, 773, and 873 K). The deposition rate of Ru was estimated using a quartz microbalance installed in the vacuum chamber. The Ru deposition amounts were determined considering the number of pulse repetitions of APD. The mass thickness was converted to monolayer thickness assuming a mass thickness of 0.3 nm was 1 ML thickness. The substrate temperatures were maintained at the specified temperatures for 30 min after deposition. Hereafter, the fabricated Ru/Ir(111) bimetallic surfaces are referred to as x K-Ru/Ir(111).

XPS and LE-ISS analyses

The fabricated Ru/Ir(111) samples were transferred to and analysed in another vacuum system equipped with X-ray photoelectron spectroscopy (XPS) and low-energy He ion scattering spectroscopy (LE-ISS) systems (analyser: PHOIBOS 1500, SPECS).[20] Mg Kα radiation (X-ray source: XR50, SPECS) was used as the X-ray source for XPS and He^+ (E_0 = 500 eV, angle of incidence: 25°, scattering angle: 115°, ion gun: OMI-0735ND-S, Omegatron) was the incident ion used for LE-ISS. The surface atomic ratios of Ir and Ru were estimated based on each deconvoluted band areas of the corresponding x K-Ru/Ir(111). In this study, because the LE-IS spectrum of clean Ir(111) collected under the above mentioned condition showed asymmetric band shape (see ESI A), the bands for x K-Ru/Ir(111) bimetallic surfaces are also deconvoluted considering the asymmetry to estimate the surface atomic ratios.

Electrochemical measurements

All electrochemical measurements were conducted at room temperature (ca. 298 K). All solutions were prepared using $HClO_4$ (Ultrapure, Kanto Chemical), $NaClO_4$ (Sendai Wako Pure Chemicals), and ultrapure water (18.2 MΩ·cm, Milli-Q). Sample transfer from the vacuum to electrochemical systems was conducted without exposure to air using a home-built transfer system.[18]

The H_2O_2 generation reaction and HOR properties were evaluated using scanning electrochemical microscopy (SECM, HV-402E, Hokuto Denko) and the experimental details were identical to those described in our previous study.[11] Briefly, SECM evaluations were conducted in air after the surface was protected by a N_2-purged solution in an N_2-purged glove box. An Ag/AgCl electrode (saturated KCl, Hokuto Denko) and Pt wire (0.05 mm diameter) were used as the reference electrode (RE) and counter electrode (CE), respectively, and the working electrode surface area was determined using an O-ring (0.062 cm^2, Karletz, DuPont) for SECM measurements.

The generation of H_2O_2 was evaluated using a substrate-generation/tip-collection (SG/TC) mode in O_2-saturated 0.1 M $HClO_4$.[21,22] The potentials denoted hereafter were converted from vs. Ag/AgCl to vs. RHE, assuming pH = 1, unless otherwise stated. The Pt ultramicroelectrode (UME) tip (ca. 20 µm diameter, Hokuto Denko) was placed ~50 µm above the sample substrate normal and the sample substrate potential (E_S) was swept using a negative-going scan of 2 mV/s at a fixed Pt UME tip potential (E_T) of 1.26 V. Both the tip current (i_T) and substrate current (i_S) were simultaneously recorded during the potential scan. H_2O_2 generation can be evaluated by the i_T induced upon the H_2O_2 generation at the sample substrate electrode surface (SG/TC mode of SECM).

In contrast, the HOR activity of the fabricated bimetallic surfaces was evaluated using the tip generation/substrate collection (TG/SC) mode in SECM in 0.01 M $HClO_4$ + 0.1 M $NaClO_4$.[23–25] The potential conversion from vs. Ag/AgCl to vs. RHE was conducted based on the cyclic voltammogram (CV) obtained for a Pt UME (ca. 25 µm diameter, Sensolytics), which was used as the tip electrode.[11] The Pt UME tip was positioned in the vicinity of the sample substrate while fixing the E_T at −0.74 V. Thereafter, the negative-going scan of E_S was conducted at 5 mV/s and the dependence of i_T against E_S was recorded (TG/SC mode of SECM).[26–28] The i_T was normalized to the normalised tip current (I_T) using the diffusion-limiting Pt UME tip current of the hydrogen evolution reaction (HER) without tip-substrate interactions ($i_{T\rightarrow\infty}$), which was recorded prior to each measurement. The value of the standard rate constant (k^0) of the HOR was determined by fitting the experimental I_T($=i_T/i_{T\rightarrow\infty}$) vs. E_S curve considering the theoretical equations.[29–31]

The H_2O_2 generation and HOR properties of the vacuum-prepared Ru/Ir(111) samples were compared with those of vacuum-cleaned Ir(111) (without Ru deposition) and vacuum-cleaned Ru(0001) and Pt(111) (both purchased from MaTeck, 99.999 %, miscut angle: <0.1°).

Results and Discussion

Surface characterization

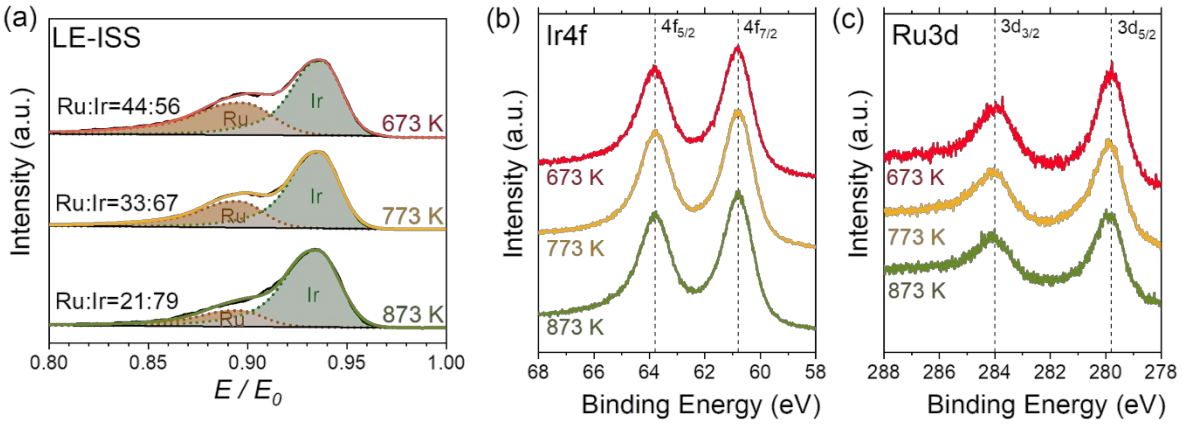

Figure 1 (a) LE-IS and XP ((b) Ir4*f* and (c) Ru3*d*) spectra obtained for *x* K-Ru/Ir(111). The dashed lines in (b) and (c) correspond to the binding energy of metallic Ir^0 or Ru^0.[34,35]

LE-ISS was used to determine the topmost surface atomic composition of Ru/Ir for the fabricated *x* K-Ru/Ir(111) samples. The recorded (a) LE-IS and corresponding XP spectra ((b) Ir 4*f* and (c) Ru3*d*) are shown in Figure 1. The LE-IS spectra show the deconvoluted bands corresponding to Ir (E/E_0 = 0.94) and Ru (E/E_0 = 0.89) (dotted lines) and the Ru/Ir surface compositions judged by each area were approximately 1:1 (*x* = 673 K), 1:2 (773 K), and 1:4 (873 K), respectively. The decreasing trend observed for the composition of Ru with increasing substrate temperature (*x*) was rationalized by the thermal diffusion of the deposited Ru atoms into the Ir(111) substrate. Theoretical calculations have proposed that Ir tends to segregate at the surface of the Ir-Ru bimetallic system[32] and similar experimental results obtained using LE-ISS have been reported in the literature.[33]

Furthermore, the atomically flat nature of the 773K-Ru/Ir(111) surface was confirmed using scanning tunnelling microscopy (STM), as shown in ESI B. In contrast, the XPS results (Figure 1 (b, c)) show that the Ir 4*f* and Ru 3*d* binding energies were almost unchanged from their corresponding pure metallic states (M^0)[34,35] irrespective of the atomic ratio of Ru:Ir. Thus, the charge transfer between Ir and Ru cannot be identified from the XP spectra (Figure 1(b),(c)).

H_2O_2 generation properties

Figure 2 shows the electrochemical current (i_T) of the Pt UME tip electrode used for H_2O_2 detection, (a), current density (j_s) of the sample substrate (working) electrode of Ru/Ir(111) (b), and normalized tip current ($i_T/|i_s|$) (c) under a negative-going potential scan of the sample substrate potential (E_s), recorded using the SG/TC mode of SECM. The results obtained for the

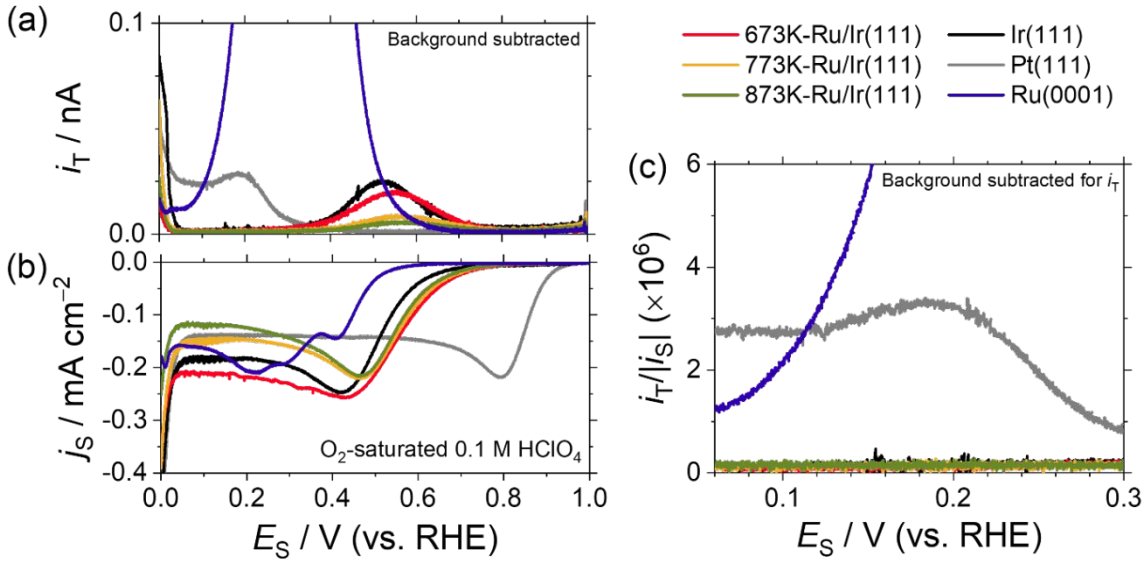

Figure 2 (a) Pt UME tip current for H_2O_2 detection (i_T), (b) sample substrate current density (j_S), and (c) tip current normalized by the substrate current ($i_T/|i_S|$) obtained using the SG/TC mode of SECM in O_2-saturated 0.1 M $HClO_4$. The minimum value of the i_T (except in the potential region with obvious noise) was subtracted as the background of i_T in (a) and (c).

vacuum-cleaned Ir(111), Ru(0001), and Pt(111) samples are also shown for reference. From the viewpoint of the development of novel anode catalysts for PEMFCs, the suppression of H_2O_2 generation in the anode potential region (0–0.3 V vs. RHE) is a top priority. However, Figure 2 shows the sharp increase in j_S, particularly in the low potential region (E_S <0.06 V) (b), which corresponds to the hydrogen evolution reaction (HER), and the influence of generated H_2 cannot be excluded for i_T. In other words, the steep increase in i_T (E_S <0.06 V) (a) contains the contribution from the HER, resulting in an overestimation of the generation of H_2O_2. Considering this, $i_T/|i_S|$ was only displayed in the range of 0.06–0.3 V (c).

H_2O_2 generation on vacuum-cleaned Ir(111) (black) is very low in the potential range of 0.06–0.3 V, and the $i_T/|i_S|$ values (c) were below the detection limit of the SG/TC mode of SECM.[11] Meanwhile, Pt(111) (grey) and Ru(0001) (blue) generate H_2O_2 in this potential region. H_2O_2 generation below ca. 0.3 V for clean Pt(111) is a well acknowledged behavior[36] and for Ru(0001), i_T markedly increases below its ORR onset potential (ca. 0.6 V) to ~0.1 V (see Figure 2 (a) and the results displayed with an appropriate graph scale in ESI C). Therefore, clean Ru(0001) generates a large amount of H_2O_2, and in a certain potential range, such as 0.1–0.5 V vs. RHE, it is even larger than that of clean Pt(111). This is in good agreement with the literature reporting the ORR behaviour of Ru/C and Pt/C.[37] Despite the H_2O_2 generation behaviour of clean Ru(0001), the suppressed H_2O_2 generation of clean Ir(111) remains almost unchanged even for the vacuum-prepared Ru/Ir(111) surfaces, as clearly shown by the i_T / $|i_S|$ vs. E_S behaviour in Figure 2 (c). Thus, when compared with clean Pt(111) and Ru(0001), the Ru/Ir(111) surfaces studied generate much less H_2O_2 throughout the potential range (0.06–0.3 V), revealing the advantages of Ir-Ru alloy surfaces in mitigating the degradation of PEM.

The aforementioned results, that is, the suppressed generation of H_2O_2 in the Ru/Ir(111) samples studied, irrespective of the surface atomic ratio of Ir:Ru, may be explained using a bifunctional mechanism. The ORR can be roughly considered as a multistep process, as shown in Scheme 1, in which superscripts * and b denote the intermediate species on the sample electrode surface and the species in the bulk solution, respectively. Scheme 1 is called the "H_2O_2-mediated pathway model," and the H_2O_2 generation evaluated using the SG/TC mode of SECM should be closely related to the balance of the kinetic parameters of sub-process S1 (intermediate H_2O_2 formation), S2 (H_2O_2 reduction to H_2O), and S3 (H_2O_2 diffusion into bulk solution).[38] Considering the ORR proceeding on Ir(111) with moderately suppressed H_2O_2 generation, particularly in the low potential region (<0.3 V), Ir(111) is further likely to promote the reduction of H_2O_2 into H_2O (S2) much faster than H_2O_2 diffusion into the bulk solution (S3). Therefore, at least on the investigated Ru/Ir(111) surfaces (i.e. surface Ru composition less than ca. 44%), it can be assumed that even if the surface Ru sites located near the Ir sites generate H_2O_2, it would be instantly reduced to H_2O on the surface Ir sites, before bulk diffusion from the reacting surface. In conclusion, the local sites of Ir on the Ru/Ir(111) surfaces will play an important role

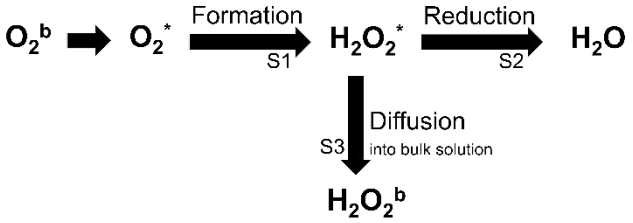

Scheme 1 Simplified model for multistep ORR process

in the suppression of H_2O_2 generation and these properties are highly desirable in anode catalysts used for PEMFCs.

HOR properties

Figure 3 (a) shows the I_T vs. E_S curves obtained for *x* K-Ru/Ir(111) recorded in a mixed solution containing 0.01 M $HClO_4$ and 0.1 M $NaClO_4$, on which the evaluation of k^0 for the HOR is based. Ideally, I_T monotonically increases as E_S increases because I_T corresponds to the reaction rate of the HOR. However, Figure 3 (a) shows the I_T values decrease above a certain potential possibly due to active site blocking by surface O/OH species.[11] Actually, the potential above which I_T decreases (ca. 0.15, 0.38, and 0.32 V for 673 K-, 773 K-, and 873 K-Ru/Ir(111), respectively) appears to roughly correspond to the onset potentials observed in CV curves (ESI D), to which the surface oxide species of Ir and/or Ru may contribute (ca. 0.25, 0.35, and 0.35 V for 673 K-, 773 K-, and 873 K-Ru/Ir(111), respectively). The curve fittings for the experimentally collected I_T vs. E_S curves were applied, excluding these potential regions. The k^0 values determined using the fitting procedure are summarized in Figure 3 (b) with the corresponding values for vacuum-cleaned Ir(111) and

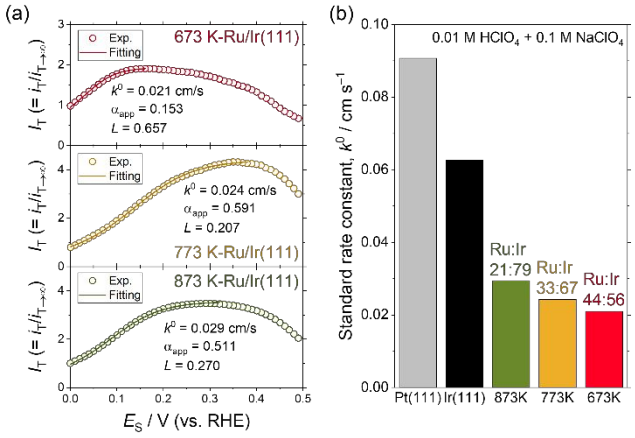

Figure 3 (a) Normalized tip current (i_T) vs. sample substrate potential (E_S) curves obtained using the TG/SC mode of SECM in a mixed solution of 0.01 M $HClO_4$ + 0.1 M $NaClO_4$ for 673 K- (red), 773 K- (yellow), and 873 K-Ru/Ir(111) (green). Both the experimental results (circles) and fitting curves (solid lines) are shown. The fitting parameters (standard rate constant: k^0, apparent transfer coefficient: α_{app}, tip-substrate distance normalized by the Pt UME tip radius: L) are also shown in the insets. (b) Estimated k_0 values obtained for *x* K-Ru/Ir(111), vacuum-cleaned Ir(111), and vacuum-cleaned Pt(111).

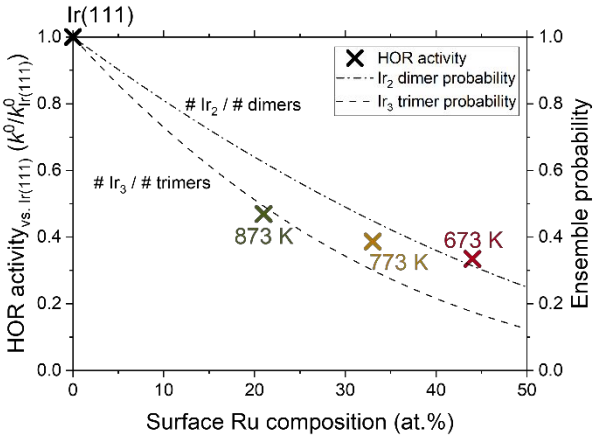

Figure 4 HOR activity observed for *x* K-Ru/Ir(111) (k^0) normalized by Ir(111) ($k^0_{Ir(111)}$) plotted against the surface Ru composition estimated using ISS measurements. The mathematically estimated probabilities of the Ir ensembles are also displayed with lines (dash-dotted: Ir_2 probability per dimer, dashed: Ir_3 probability per trimer).

Pt(111).[11] Notably, the HOR activity of clean Ru(0001) in perchloric acid solution was very low;[39,40] the exchange current density has been reported to be ~1/100 of that of clean Pt(111) because of its strong binding to the adsorbed hydrogen atoms (H_{ad}).[39] All of the samples exhibit lower k^0 values than clean Ir(111) and lower annealing temperatures, i.e., a higher surface Ru composition causes smaller k^0 values. This result was consistent, in general, with previous DFT calculations used to estimate the HOR activity of Ir-Ru alloyed surfaces, as judged from the hydrogen binding energy.[17] By contrast, the Pak's group have reported that Ir-Ru/C with relatively high Ru contents ($IrRu_4$ or $IrRu_2$) exhibits enhanced HOR activity.[12–16] This may be explained by the possibility of Ir-rich shell formation, which was mentioned by the author.[12] Furthermore, according to the DFT calculations, the Ir shell–Ru-rich core nanostructure can promote the HOR.[17] Although the Ir shell–Ru core model structure, e.g. Ir/Ru(0001), which is fully covered by monolayer-thick Ir, was not tested in this study, the formation of the Ir-rich surface may be effective in achieving the high HOR activity of the Ir-Ru bimetallic system.

To obtain deeper insights into the relationship between the HOR activity and surface atomic structures of the Ru/Ir(111) bimetallic surfaces, the obtained standard rate constants were plotted in Figure 4 against the topmost surface Ru compositions determined using LE-ISS. Furthermore, Figure 4 also shows the local probability of the atomic ensembles of Ir, e.g., dimer sites (Ir_2; dash-dotted) and trimer sites (Ir_3; dashed): the ensemble probabilities were calculated under assumption of randomly solute Ir and Ru atoms. The calculation procedures used for the probabilities of the ensembles are described in detail in ESI E, and the results obtained for the Ir-Ru sites, e.g., dimer (Ir_2, IrRu, and Ru_2) and trimer (Ir_3, Ir_2Ru, $IrRu_2$, and Ru_3) sites are summarized in ESI F. Figure 4 clearly shows the SECM-estimated k^0 values were in line with the local probability for surface Ir dimer and trimer ensembles, rather than with the probability of other ensembles with Ir-Ru sites (IrRu, Ru_2, Ir_2Ru, $IrRu_2$, and Ru_3, see ESI F). Therefore, for the Ru/Ir(111) samples used in this study, it can be considered that the pure Ir surface sites, such as Ir_2 and/or Ir_3, primarily contribute to the catalysis of the HOR. In other words, the decreased HOR activity of the Ru-enriched surfaces can be attributed to the decrease in the Ir ensembles due to the neighbouring Ru atoms. Therefore, formations of the Ir ensemble sites could be effective to develop a novel Ir-Ru alloy catalyst for PEMFC anode. Recently, dimer[41] and trimer[42,43] formations at topmost surface of nano-sized catalyst particles were reported as a novel catalyst design strategy, and such techniques could be utilized. However, it should be noted that change in electronic states through the formation of the ensemble sites, which is discussed in the literatures,[41-43] cannot be confirmed by the present XP spectra (Figure 1 (b), (c)).

Interestingly, Ishikawa et al. reported the HOR activity of Ru-Ir/C was enhanced by the Ru-Ir pair sites in an alkaline solution.[44] The results reported in an alkaline solution was opposite to the present results obtained in an acidic solution. This discrepancy may be explained by the different HOR mechanisms that occur under acidic and alkaline conditions. The HOR in an alkaline solution ($H_2 + 2OH^- \rightarrow 2H_2O + 2e^-$) includes the reaction between OH^- species and hydrogen species, and Ru atoms interacted with the OH^- species due to its higher oxophilicity than Ir.[44] However, the HOR in an acidic environment ($H_2 \rightarrow 2H^+ + 2e^-$) did not, evidently, include the reaction with the OH^- species and thus, the HOR enhancement mechanism by the Ir-Ru pair probably did not work in an acidic solution.

Conclusions

The H_2O_2 generation and HOR properties of well-defined Ru/Ir(111) surfaces have been investigated in an acidic solution using SECM. The *x* K-Ru/Ir(111) surfaces were prepared via APD of 1 ML-thick Ru on Ir(111) substrates by varying the substrate temperature (*x* = 673, 773, and 873 K), aiming to fabricate the bimetallic surfaces with different surface atomic ratios through thermal inter-diffusion of the APD Ru and Ir atoms of (111) substrate. The LE-ISS estimated topmost surface Ru:Ir atomic ratios were ca. 1:1, 1:2, and 1:4 for the 673, 773, and 873 K-Ru/Ir(111), respectively. H_2O_2 generation by the prepared Ru/Ir(111) was evaluated using the SG/TC mode of SECM. Although clean Ru(0001) generated a large amount of H_2O_2, all of the Ru/Ir(111) surfaces markedly suppressed the generations of H_2O_2 in the potential region of 0.06–0.3 V vs. RHE, which is comparable to clean Ir(111), irrespective of the Ru:Ir surface composition. The results suggest that even when the surface local Ru sites generate H_2O_2, it would be instantaneously reduced to H_2O by adjacent Ir sites, resulting in the suppressed generation of H_2O_2. The HOR activity (standard rate constant, k^0) estimated using the TG/SC mode of SECM for the corresponding Ru/Ir(111) samples followed the order: clean Ir(111) > 873 K-Ru/Ir(111) > 773 K-Ru/Ir(111) > 673 K-Ru/Ir(111), and the HOR was deactivated upon increasing the surface composition of Ru. Furthermore, the estimated k^0 values were well correlated with the surface Ir ensemble sites of Ir_2 and Ir_3,

which were calculated by assuming random solution of the surface Ir and Ru atoms. The result indicates that the pure Ir sites strongly contribute to the HOR on the Ru/Ir(111) surface. In conclusion, the surface Ir sites of Ir-Ru bimetallic alloy surfaces should determine the catalytic properties (H_2O_2 generation and HOR), which are important for the development of novel PEMFC anode catalysts.

Author Contributions

KH was involved in investigation, visualization, writing original draft and editing. KK, TT and RS were involved in investigation. NT was involved in investigation, supervision, review and editing. TW was involved in conceptualization, funding acquisition, project administration, supervision, review and editing. All authors reviewed the manuscript, and approved the final report.

Conflicts of interest

There are no conflicts to declare.

Acknowledgements

This research was supported by the New Energy and Industrial Technology Development Organization (NEDO) of Japan, JSPS KAKENHI Grant Number JP21H01645 (TW), and JST SPRING Grant Number JPMJSP2114 (KH).

Notes and references

1 O. Z. Sharaf and M. F. Orhan, *Renew. Sustain. Energy Rev.*, 2014, **32**, 810–853.
2 R. Borup, J. Meyers, B. Pivovar, Y. S. Kim, R. Mukundan, N. Garland, D. Myers, M. Wilson, F. Garzon, D. Wood, P. Zelenay, K. More, K. Stroh, T. Zawodzinski, J. Boncella, J. E. McGrath, M. Inaba, K. Miyatake, M. Hori, Z. Ogumi, S. Miyata, A. Nishikata, Z. Siroma, Y. Uchimoto, K. Yasuda, K. Kimijima, and N. Iwashita., *Chem. Rev.*, 2007, **107**, 3904–3951.
3 M. Inaba, T. Kinumoto, M. Kiriake, R. Umebayashi, A. Tasaka, and Z. Ogumi, *Electrochim. Acta*, 2006, **51**, 5746–5753.
4 T. Kinumoto, M. Inaba, Y. Nakayama, K. Ogata, R. Umebayashi, A. Tasaka, Y. Iriyama, T. Abe, and Z. Ogumi, *J. Power Sources*, 2006, **158**, 1222–1228.
5 E. Endoh, *ECS Trans.*, 2008, **16**, 1229–1240.
6 M. Zatoń, B. Prélot, N. Donzel, J. Rozière, and D. J. Jones, *J. Electrochem. Soc.*, 2018, **165**, F3281–F3289.
7 S. M. Stewart, D. Spernjak, R. Borup, A. Datye, and F. Garzon, *ECS Electrochem. Lett.*, 2014, **3**, F19–F22.
8 G. Shi, D. A. Tryk, T. Iwataki, H. Yano, M. Uchida, A. Iiyama, and H. Uchida, *J. Mater. Chem. A*, 2020, **8**, 1091–1094.
9 E. Antolini, *ChemElectroChem*, 2014, **1**, 318–328.
10 J. Durst, C. Simon, F. Hasché, and H. A. Gasteiger, *J. Electrochem. Soc.*, 2015, **162**, F190–F203.
11 K. Hayashi, T. Tomimori, Y. Chida, N. Todoroki, and T. Wadayama, *J. Phys. Chem. C*, 2021, **125**, 21481–21487.
12 E. You, M. Min, S.-A. Jin, T. Kim, and C. Pak, *J. Electrochem. Soc.*, 2018, **165**, F3094–F3099.
13 S. W. Lee, B. H. Lee, T.-Y. Kim, C. Baik, M. S. Kim, G. S. Chai, and C. Pak, *Catal. Commun.*, 2019, **130**, 105758.
14 T. Y. Kim, S. W. Lee, and C. Pak, *J. Ind. Eng. Chem.*, 2020, **85**, 87–93.
15 S. W. Lee, B. Lee, C. Baik, T. Y. Kim, and C. Pak, *J. Mater. Sci. Technol.*, 2021, **60**, 105–112.
16 C. Pak, S. W. Lee, C. Baika, B. H. Lee, D. J. You, and E. You, *Chinese Chem. Lett.*, 2019, **30**, 1186–1189.
17 J. R. De Lile, A. Bahadoran, Q. Liu, S. W. Lee, C. Pak, J. Zhang, and S. G. Lee, *Appl. Surf. Sci.*, 2021, **545**, 149002.
18 T. Wadayama, N. Todoroki, Y. Yamada, T. Sugawara, K. Miyamoto, and Y. Iijama, *Electrochem. Commun.*, 2010, **12**, 1112–1115.
19 T. Wadayama, H. Yoshida, K. Ogawa, N. Todoroki, Y. Yamada, K. Miyamoto, Y. Iijima, T. Sugawara, K. Arihara, S. Sugawara, K. Shinohara, *J. Phys. Chem. C*, 2011, **115**, 18589-18596.
20 N. Todoroki, Y. Iijima, R. Takahashi, Y. Asakimori, and T. Wadayama, *J. Electrochem. Soc.*, 2013, **160**, F591–F596.
21 C. M. Sánchez-Sánchez and A. J. Bard, *Anal. Chem.*, 2009, **81**, 8094–8100.
22 A. Kishi, S. Shironita, and M. Umeda, *J. Power Sources*, 2012, **197**, 88–92.
23 J. Zhou, Y. Zu, and A. J. Bard, *J. Electroanal. Chem.*, 2000, **491**, 22–29.
24 C. G. Zoski, *J. Phys. Chem. B*, 2003, **107**, 6401–6405.
25 Y. C. Weng and C. T. Hsieh, *Electrochim. Acta*, 2011, **56**, 1932–1940.
26 C. G. Zoski, C. R. Luman, J. L. Fernández, and A. J. Bard, *Anal. Chem.*, 2007, **79**, 4957–4966.
27 M. A. Brites Helú and J. L. Fernández, *J. Electroanal. Chem.*, 2017, **784**, 33–40.
28 K. Jambunathan, B. C. Shah, J. L. Hudson, and A. C. Hillier, *J. Electroanal. Chem.*, 2001, **500**, 279–289.
29 S. Amemiya, N. Nioradze, P. Santhosh, and M. J. Deible, *Anal. Chem.*, 2011, **83**, 5928–5935.
30 C. Lefrou and R. Cornut, *ChemPhysChe*m, 2010, **11**, 547–556.
31 R. Cornut and C. Lefrou, *J. Electroanal. Chem.*, 2008, **621**, 178–184.
32 A. V. Ruban, H. L. Skriver, and J. K. Nørskov, *Phys. Rev. B - Condens. Matter Mater. Phys.*, 1999, **59**, 15990–16000.
33 N. Danilovic, R. Subbaraman, K. C. Chang, S. H. Chang, Y. Kang, J. Snyder, A. P. Paulikas, D. Strmcnik, Y. T. Kim, D. Myers, V. R. Stamenkovic, and N. M. Markovic, *Angew. Chemie. Int. Ed.*, 2014, **53**, 14016–14021.
34 S. J. Freakley, J. Ruiz-Esquius, and D. J. Morgan, *Surf. Interface Anal.*, 2017, **49**, 794–799.
35 D. J. Morgan, *Surf. Interface Anal.*, 2015, **47**, 1072–1079.
36 N. M. Markovic, H. A. Gasteiger, and P. N. Ross, *J. Phys. Chem.*, 1995, **99**, 3411–3415.
37 T. J. Schmidt, U. A. Paulus, H. A. Gasteiger, and R. J. Behm, *J. Electrochem. Soc.*, 2000, **147**, 2620–2624.
38 F. Yin, Y. Liu, S. Wang, C. Wang, and H. Liu, *Electrochim. Acta*, 2019, **313**, 378–388.
39 M. P. Mercer and H. E. Hoster, *Electrocatalysis*, 2017, **8**, 518–529.
40 H. Inoue, J. X. Wang, K. Sasaki, and R. R. Adzic, *J. Electroanal. Chem.*, 2003, **554–555**, 77–85.
41 H. Li, S. Dai, D. Bhalothia, J. P. Chou, A. Hu, and T. Y. Chen, *Phys. Chem. Chem. Phys.*, 2021, **23**, 1822-1834.
42 H. Li, K. W. Wang, T. Y. Chen, A. Hu, J. P. Chou, and T. Y. Chen, *Phys. Chem. Chem. Phys.*, 2021, **23**, 18012-18025.
43 S. Dai, J. P. Chou, K. W. Wang, Y. Y. Hsu, A. Hu, X. Pan, and T. Y. Chen, *Nature Commun.*, 2019, **10**, 1-10.
44 K. Ishikawa, J. Ohyama, K. Okubo, K. Murata, and A. Satsuma, *ACS Appl. Mater. Interfaces*, 2020, **12**, 22771–22777.